Accepted Manuscript

Insights from atomistic models on loop nucleation and growth in *α*-Fe thin films under Fe^+ 100□keV irradiation

J.P. Balbuena, M.J. Aliaga, I. Dopico, M. Hernández-Mayoral, L. Malerba, I. Martin-Bragado, M.J. Caturla

PII: S0022-3115(18)31681-7

DOI: https://doi.org/10.1016/j.jnucmat.2019.04.030

Reference: NUMA 51578

To appear in: *Journal of Nuclear Materials*

Received Date: 10 December 2018

Revised Date: 10 April 2019

Accepted Date: 22 April 2019

Please cite this article as: J.P. Balbuena, M.J. Aliaga, I. Dopico, M. Hernández-Mayoral, L. Malerba, I. Martin-Bragado, M.J. Caturla, Insights from atomistic models on loop nucleation and growth in *α*-Fe thin films under Fe^+ 100□keV irradiation, *Journal of Nuclear Materials* (2019), doi: https://doi.org/10.1016/j.jnucmat.2019.04.030.

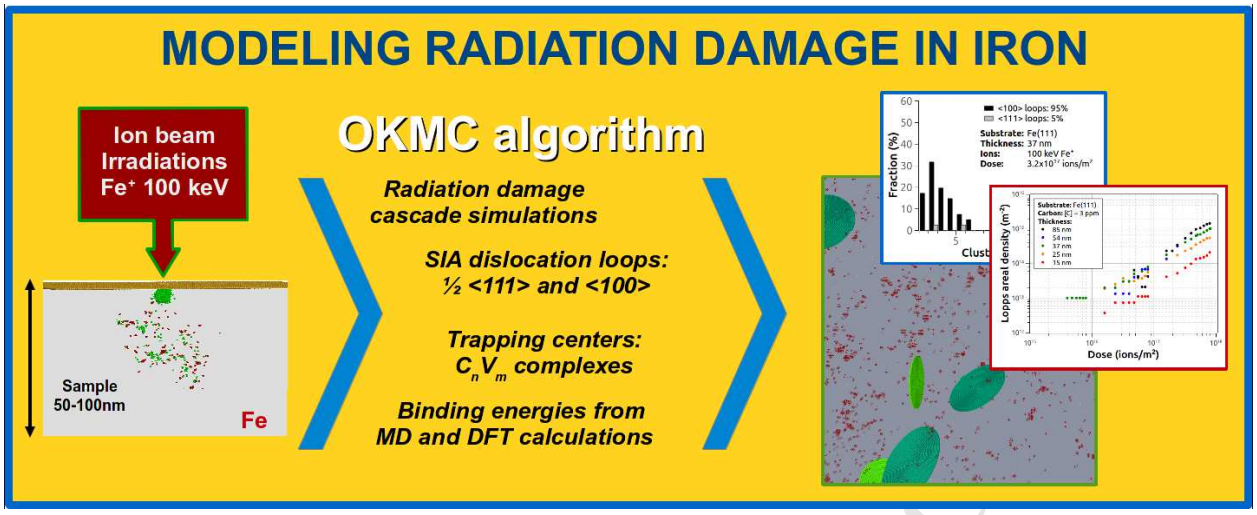

Insights from atomistic models on loop nucleation and growth in α-Fe thin films under Fe^+ 100 keV irradiation

J.P. Balbuena[a], M.J. Aliaga[a], I. Dopico[b], M. Hernández-Mayoral[c], L. Malerba[d], I. Martin-Bragado[e], M.J. Caturla[a,*]

[a] *Departamento de Física Aplicada, Universidad de Alicante, E-03690 Alicante, Spain*
[b] *Universidad Politécnica de Madrid, ETS de Ingenieros de Caminos, E-28040 Madrid, Spain*
[c] *CIEMAT, Departamento de Tecnología, División de Materiales Estructurales, E-28040 Madrid, Spain*
[d] *SCK-CEN, Nuclear Material Science Institute, B-2400 Mol, Belgium*
[e] *UCAM, Universidad Católica de Murcia, Campus de los Jerónimos, E-03017 Murcia, Spain*

Abstract

The question of how loops nucleate and grow in α-Fe under irradiation is addressed using object kinetic Monte Carlo with parameters from molecular dynamics and density functional theory calculations. Two models are considered for the formation of <100> loops, both based on recent atomistic simulations. In one model <100> loops are formed by the interaction between $\frac{1}{2}$<111> loops. In a second model small interstitial clusters, nucleated in the collision cascade, can grow as <100> or $\frac{1}{2}$<111> loops. Comparing results from the calculations to experimental measurements of loop densities, ratios and sizes produced by Fe^+ 100 keV irradiation of UHP Fe thin films at room temperature, the validity of the models is assessed. For these experimental conditions, the reaction model does not seem to be very efficient in the production of <100> loops due to the fast recombination of $\frac{1}{2}$<111> loops to surfaces. Therefore, in our thin film simulations (at very low carbon concentrations) most <100> loops are a result of the nucleation model. In bulk simulations this effect could change since the probability of interactions between $\frac{1}{2}$<111> loops would increase. Moreover, simulations show that total visible cluster concentration depends strongly on sample thickness and carbon content, while crystal orientation does not seem to have a significant role. Finally, the ratio of <100> to $\frac{1}{2}$<111> visible clusters changes with increased carbon concentration.

Keywords: Monte Carlo simulation, Ion irradiation, Iron, Irradiation effect, In situ transmission electron microscopy

1. Introduction

An outstanding question in the field of radiation damage effects in Fe-based alloys is how loops nucleate and grow under irradiation. Experimentally, it is well known since the 1960s that two types of loops are formed: <100> and $\frac{1}{2}$<111> [1–7]. However,

*Corresponding author. Tel. +34 965903400 ext: 2056
Email address: mj.caturla@ua.es (M.J. Caturla)

the character (vacancy or self-interstitial), concentration, ratio and sizes of these loops differs considerably depending on the experimental conditions. Moreover, the reason why both families of loops are observed is still not completely clear. Elasticity theory and simulations predict that $\frac{1}{2}$<111> loops have lower energies than <100> loops and should be the dominant defect at low temperatures [8, 9]. As temperature increases, <100> loops become more stable due to the magnetic transition that iron experiences at 770°C [10]. On the other hand $\frac{1}{2}$<111> loops are highly mobile according to computer simulations [11–13] in what could be considered as an athermal migration [14]. Therefore, these clusters should quickly migrate to sinks such as dislocations, grain boundaries or surfaces and not be observed in the bulk.

Several explanations have been given within the past few years for the presence of both <100> and $\frac{1}{2}$<111> loops, coming from computer simulations as well as detailed experimental measurements. The observation of $\frac{1}{2}$<111> loops despite their fast migration is explained by the presence of traps, that slow down the motion of these clusters. Experiments performed by Arakawa et al. [15] have shown that the migration energy of these loops is closer to 1 eV than to the 0.1 eV values obtained from atomistic simulations [11–13]. Several candidates have been proposed as possible traps for these clusters [16–19]. MD simulations have shown that vacancies can be weak traps for self-interstitial loops [18], but binding energies are too low to explain trapping at room temperature. Carbon, that is always present even if in very low concentrations, is often considered to affect the mobility of these loops [16, 17]. This interaction could be aided by vacancies, forming C-vacancy complexes that can then trap self-interstitial loops [18, 19]. Moreover, other interstitial atoms that form stable clusters with vacancies, namely N and O [20], or He [21] may have a similar effect. Substitutional impurities, such as P, may also interact with gliding loops and slow down their motion [22]. In addition, the interaction of these loops among themselves could also form junctions that make them immobile, as assumed in some models [16].

The presence of <100> loops has been more difficult to elucidate and it is still an open question. These defects should only become dominant at high temperature, but in fact they can be created and observed experimentally also at temperatures as low as 140 K. Thus, the inversion of stability between the two classes of loops with increasing temperature is not a sufficient criterion to explain the existence of <100> loops. There are currently two main explanations, both based on computer simulations. Marian et al. [23] proposed the formation of these loops from reactions between $\frac{1}{2}$<111> loops, supported by molecular dynamics (MD) simulations and based on the earlier work of Masters [1]. Later on, Xu et al. [24] obtained the formation of complete <100> loops by reactions between $\frac{1}{2}$<111>, using different interatomic potentials in MD [25–27] together with advanced kinetic Monte Carlo calculations. More recently, a new possible mechanism of formation of these loops, already speculatively discussed in [28], has been proposed based on the work of Marinica et al. [27]: <100> loops could grow from small immobile clusters, C15 clusters [29] originally observed in MD simulations by Bacon et al. [11], that are characterized by a complex structure, not defined as a collection of parallel dumbbells or crowdions.

Microstructure evolution in irradiated Fe has been simulated with kinetic Monte Carlo and rate theory models by several groups [16, 19, 30–32]. However, except for a recent work by Terentyev and Martin-Bragado for electron irradiation [19], no distinction is made between the different types of self-interstitial clusters, and the ratios between

<100> and $\frac{1}{2}$<111> loops are not followed. In this work, we have gathered the existing information about cluster stabilities and mobilities together with the different models for growth of loops in Fe explained above. All these parameters and reactions have been implemented in a kinetic Monte Carlo model and have been used to simulate irradiation at low energies, 100 keV, in UHP Fe thin films at room temperature. A model for the interaction of carbon with vacancies and self-interstitials based on the work of Serra [18] and Terentyev [33, 34] is used to introduce a mechanism for the trapping of loops.

Results obtained from the simulations in terms of defect densities and sizes have been contrasted with corresponding experimental measurements [6]. These experiments have been performed by Yao et al. [6] as a series of systematic in-situ transmission electron microscopy (TEM) studies of irradiation of thin films of Fe and Fe-Cr alloys with heavy ions. Fe^+ and Xe^+ ions of energies of 100 keV and 150 keV were used for irradiations both at room temperature and 300°C. Loops were first observed at doses above $10^{16}m^{-2}$ and both <100> and $\frac{1}{2}$<111> loops could be identified, with a much higher proportion of <100> loops, especially for those foils consisting of pure Fe. In this work we focus on the results for room temperature Fe samples irradiated with 100 keV Fe^+ ions. The comparison between experiments and simulations allows us to extract some conclusions about the most probable mechanism for loop growth under these irradiation conditions.

2. Model parametrization

We have used our database of 100 keV cascades of Fe irradiation of Fe thin films. MD simulations were used to reproduce the resulting damage after ion implanation by sending an Fe ion with the energy of interest towards an Fe thin film. This resulted in damage with characteristics very different from bulk irradiation. Firstly, an imbalance between the number of vacancies and interstitials was found that was attributed to the faster diffusion of SIAs that escape to the surface where they stay as ad-atoms [35]. Secondly, vacancy clusters are larger than those obtained in bulk cascades while self-interstitial clusters are smaller. The resulting cascades were stored so they could be randomly sampled when called from the Object Kinetic Monte Carlo code MMonCa, developed by I. Martin-Bragado et al. [36]. Each cascade of point defects is finally inserted while running our simulations and centered in a random XY position to mimic homogeneous ion irradiation of the surface. The simulation cells we have used are also thin films whose thicknesses range from 15 to 85 nm, reproducing the different thicknesses of the thinned sample used in the experimental work of Yao et al. [6]. A compromise between simulation time and computational resources usage has been chosen to select the area of the simulation cells. Accordingly, these areas range from 516×516 nm^2 for 15 nm thick samples, to 216×216 nm^2 for 85 nm, resulting in simulation box volumes of about 4×10^6 nm^3 for all the samples. The temperature in the simulation box is set to 294.15 K, at which <100> loops are considered immobile as shown in Table 1 following MD calculations [23].

In our code, small self-interstitial atom (SIA) clusters up to a size of 4 SIA are mobile with migration energies given in Table 1, obtained from density functional theory (DFT) calculations [37]. These self-interstitial clusters are considered to move in three dimensions. From size 5, as obtained in [38] from DFT calculations, the orientation of the clustered dumbbells changes from <110> to <111> as it is energetically favoured.

Then, the formation of <100> loops is implemented in our code according to one of these two models:

Reaction model: In this model all interstitial clusters above size 4 transform into $\frac{1}{2}$<111> loops with migration energies given also in Table 1 and obtained from classical molecular dynamics simulations [13]. These loops move one-dimensionally, unlike vacancies or smaller SIA clusters. According to this model, the interaction between $\frac{1}{2}$<111> loops might result in the formation of <100> loops if two specific conditions are simultaneously satisfied: a) the sum of their Burger's vector gives as a result a Burger's vector belonging to the family of <100> directions, and b) the sizes of both interacting loops are larger than a threshold (about 20 according to Marian et al. [23, 39]), the influence of which was studied, and both are about the same size (within a 5% margin of difference, as suggested by the simulations of Marian et al. [23, 39]). If the former conditions are not fulfilled, then the resulting loop becomes a bigger $\frac{1}{2}$<111> loop with its Burger's vector oriented along the direction of the bigger interacting loop. The minimum size of the resulting <100> loop that can be formed under these conditions is one of the parameters that has been evaluated in this work. Once the <100> loops are formed, they can grow by the incorporation of small interstitial clusters (<5 SIA), by capturing smaller $\frac{1}{2}$<111> loops and by coalescence with other immobile <100> loops or immobilized smaller C-$\frac{1}{2}$<111> loops. In case of interacting with a larger SIA cluster, the Burger's vector of the resulting dislocation loop is the one corresponding to the larger SIA cluster.

Nucleation model: In this model $\frac{1}{2}$<111> and <100> loops can be formed independently. SIA clusters from size 5 can either transform into $\frac{1}{2}$<111> loops or into <100> loops with a given ratio. This ratio was initially taken as 5%, following the idea of Marinica et al. [27] that considers this as the ratio of immobile C15 clusters formed in a collision cascade, and assuming that all these clusters will grow into <100> loops. The influence of this ratio has also been evaluated and discussed in the next section. Once formed, both types of loops can grow following the same conditions as described for the reaction model.

In both models $\frac{1}{2}$<111> loops can be stopped by the interaction with carbon-vacancy and carbon-interstitial clusters following the work of Terentyev and Martin-Bragado [19]. These immobile C-$\frac{1}{2}$<111> loops can then grow by addition of SIA clusters < 5 and mobile $\frac{1}{2}$<111> loops of similar size. Also, <100> vacancy loops have been included in the models. The equation derived by Gilbert in [40] has been used for the binding energy of the vacancies in the loop. In this equation the radius of the loop is calculated using the size and the density of the loop. For the binding energies of $V_{n>4}$ and $I_{n>4}$ clusters, we have used the usual extrapolation law [37] $E_b(n) = E_f + [E_b(2) - E_f][n^{2/3} - (n-1)^{2/3}]/(2^{2/3}-1)$. For the smaller species up to 4, DFT values have been used [37]. These small vacancy clusters are considered mobile, with a 3D mobility, while larger vacancy clusters are immobile. Table 1 summarizes the most important parameters of the species involved. These parameters are also used to calculate point defects emission rates from clusters, as described elsewhere [36].

One specific feature of MMonCa is that the location of all defects in a cluster are explicitly defined. This provides more flexibility for the definition of capture volume of a defect, since it is not restricted to a sphere, but it is given by the shape of the cluster defined by the defects that form that cluster. The interaction between two clusters will then happen when the distance between two defects belonging to each cluster is smaller than, or equal to, the specified capture distance. The capture distance for all defects as

Table 1: Type of defect, migration and binding energies of the objects defined in our OKMC model. Last column corresponds to the dimensionality of migration. For the mono-defects, V and I, the formation energy is taken from ab initio calculations [37], $E_f(V) = 2.07$ eV and $E_f(I) = 3.77$ eV.

Defect	Migration barrier (eV)	Binding energy (eV)	Migration type
I	0.34		3D
I_2	0.42	0.80	3D
I_3	0.43	I to I_2 0.92	3D
I_4	0.43	I to I_3 1.64	3D
$\frac{1}{2}$<111> loop: $I_{n\geq 5}$	0.05	As in ref. [41]	1D
<100> loop: $I_{n\geq 5}$	Immobile	As in ref. [41]	–
V	0.67		3D
V_2	0.54	0.3	3D
V_3	0.43	V to V_2 0.37	3D
V_4	0.62	V to V_3 0.62	3D
$V_{n\geq 5}$	Immobile	As in ref. [41]	–
<100> loop: $V_{n\geq 5}$	0.5	As in ref. [40]	1D*
C	0.86		3D
$CI_{n\geq 5}$	Immobile	C to I_n $\{0.4 - 0.66\}^\dagger$	–
$C_{m\geq 2}I_{n\geq 5}$	Immobile	C to $C_{m-1}I_n$ 0.70	–
CV	Immobile	0.68	–
CV_2	1.1	C to CV 1.01	3D
C_mV_n	Immobile	As in ref. [34]	–

* <100> vacancy clusters introduced into OKMC as obtained from MD cascade simulations.

† E_{bind} = 0.4 eV (n<20), 0.45 eV (20<n<50), 0.50 eV (50<n<90), 0.66 eV (n>90)

well as for interfaces has been set equal to 1 times the lattice parameter of BCC iron: 0.287 nm.

As mentioned above, the database of damage created by the collision cascade used for these simulations has been obtained from molecular dynamics simulations with the specific experimental conditions: 100 keV Fe^+ ion irradiation of Fe substrates [35]. Those simulations showed that the damage distribution for this particular irradiation energy is very different from that in the case of bulk irradiation. Particularly, <100> vacancy loops with more than 400 defects were produced. These loops are always located within a few layers from the surface. Vacancy <100> loops can only be created in cascades, based on the input from molecular dynamics simulations. Thus, the only vacancy clusters that are considered as loops in the kinetic Monte Carlo calculations are those that come from the cascades, while all other vacancy clusters are considered as voids. In principle, <100> loops have a very low mobility [23] and are thus often considered immobile (for example in Table 1 the <100> loops of interstitial nature are considered immobile). However, if we consider that also all <100> vacancy loops formed in the MD simulations do not migrate or recombine with the surface, then the concentration of <100> loops is extremely high and in complete disagreement with the experimental, that observe these type of loops occasionally and always at very low doses and close to the surface. Therefore, if we accept the defect size distribution obtained from MD, there must be a mechanism of recombination of the <100> loops located very close to the surface, which in this case are all vacancy type. The interaction of these dislocation loops with surfaces can be modelled using an elastic approach [42] or dislocation dynamics [43], however, since elastic interactions were not implemented so far in this model, we propose that this recombination is due to image forces as discussed in Ref. [44] and include this effect in the OKMC code by assigning a migration energy of 0.5 eV, strictly only in the case of <100> loops of vacancy nature introduced directly by cascades, so that they can recombine with the surface.

The conditions for the irradiation follow those in the experiment by Yao et al. [6]. Simulations are performed at room temperature, with a dose rate of 8×10^{14} ions/m^2/s in pure Fe and Fe with different carbon concentrations. Foil orientations along (100) and (111) planes are studied. The concentration of defects as a function of dose is analyzed under different conditions of foil orientation, foil thickness, carbon concentration as well as the type of model for loop growth: the reaction and the nucleation model, as explained above. In order to compare with experimental measurements of defect densities obtained by TEM it is important to take into account the minimum visible size resolvable experimentally. The authors mentioned in their work that they could resolve dislocation loop sizes of about 1.5 nm in diameter, which corresponds to 30 SIA [45, 46]. So this is the value used as visibility threshold in this work and therefore as the lower limit in size for the first bin (i.e.: 1-2 nm) of all the represented histograms.

3. Results

Figures 1a and 1b show the concentration of visible defects as a function of irradiation dose obtained from the two models for loop growth described above, considering each model independently. In these simulations no carbon was included, therefore, due to the fast migration of $\frac{1}{2}$<111> loops to the surface, all remaining loops are of <100> type. These calculations are done for test structures consisting of thin films of 270×270×50

nm^3 and crystal orientation Fe(100). The Fe ion flux was set to 8×10^{14} ions/m^2/s and the maximum dose achieved was 1×10^{18} ions/m^2.

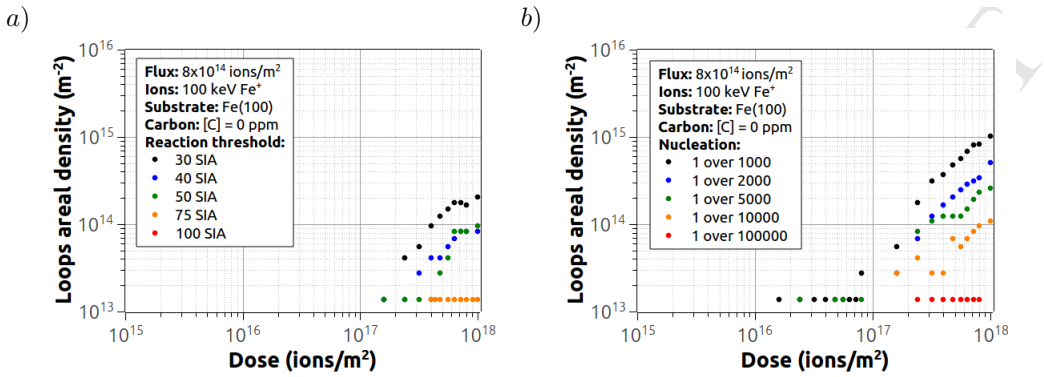

Figure 1: Areal density of visible SIA dislocation loops as a function of dose for several cases of each model. Plot (a) shows the results of the reaction model. Different values of the minimum size of the resulting <100> loop after the collision of two SIA $\frac{1}{2}$<111> SIA loops are considered. Plot (b) shows the results of the nucleation model after changing the chances of small SIA loops to turn, as they grow ($\geq$ 5 SIA), into either immobile <100> or mobile $\frac{1}{2}$<111>, being the former the least favorable case. The simulation volume in both cases was set to $270\times270\times50$ nm^3.

Both models have one parameter that could change the outcome of the evolution of defects. In the case of the reaction model this parameter is the threshold in size considered for the formation of a <100> loop after the reaction of two $\frac{1}{2}$<111> loops, while in the case of the nucleation model it is the ratio of transformations of small SIA clusters (exceeding 4 SIA) into <100> loops, considered to be formed within the collision cascade. The rest of the transformations result in $\frac{1}{2}$<111> loops. Concerning the first parameter, according to the work of Marian [23] as well as the work of Xu [24], in order to form a <100> loop the reacting clusters must have similar sizes. Marian [23, 39] also states that loops must have at least ~20 defects each in order to form a <100> loop. We have performed calculations for different threshold sizes of the $\frac{1}{2}$<111> loops that would give rise to the formation of a <100>, presented in Figure 1a) for minimum resulting sizes between 30 and 100 self-interstitials (or 15 and 50 self-interstitials on each interacting loop). This figure shows that, as the minimum size for loop formation increases, the concentration of <100> loops decreases, according to expectations. This model predicts a very low concentration of <100> for all sizes studied and the irradiation conditions considered in these simulations. Even for the smallest threshold (30 SIA), the concentration at a dose of 1×10^{18} ions/m^2 is only around 2×10^{14} loops/m^2. This is the result of the very restrictive conditions to form <100> loops through this mechanism, particularly the fact that the sum of the Burger's vectors must be the appropriate one. Consequently, for thin films most of the $\frac{1}{2}$<111> reach the surface before interacting with each other to form <100> loops. Therefore, under the conditions simulated here, we do not expect a significant contribution of this mechanism in the formation of <100> loops.

Turning to the nucleation model and the seed ratio of <100> and $\frac{1}{2}$<111> loops, according to the work of Marinica [27], about 5% of the clusters produced in a collision cascade are of C15 type. However, not necessarily all these clusters are going to evolve

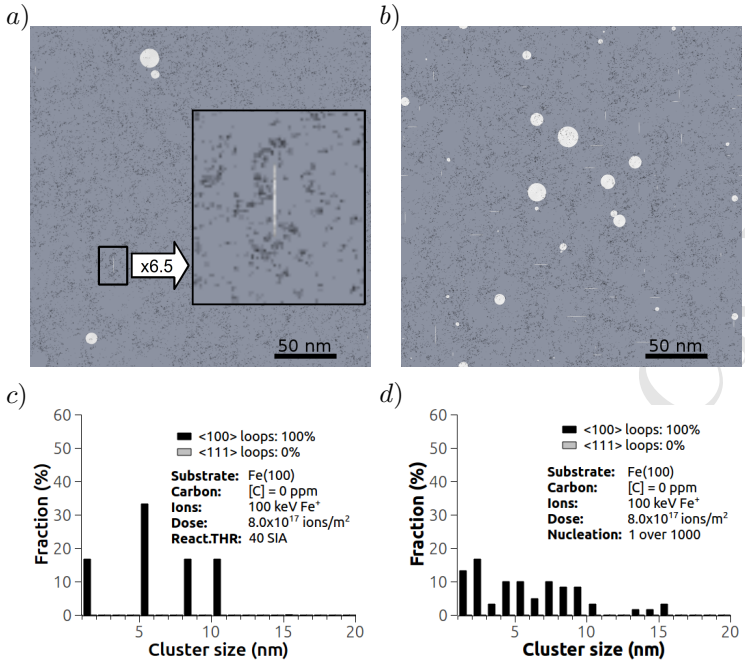

Figure 2: Simulation results for reaction and nucleation models after a radiation dose of 8.0×10^{17} ions/m^2. Image (a) corresponds to the 40 SIA threshold of the reaction model, whereas its loop size distribution is represented in (c). Image (b) corresponds to the formation of one <100> every 1000 transitions of small SIA clusters to dislocation loops in the nucleation model. The loop size distribution is represented in figure (d). Only one active model for <100> loops (represented as disks formed by white dots) formation is enabled at a time in these simulations. A zoomed detail of a dislocation loop perpendicular to the top view representation is also featured in figure (a).

to <100> loops. Therefore, the ratio of small defects that are considered to transform into $\frac{1}{2}$<111> loops or <100> loops is a free parameter in this model. Figure 1b shows the dependence of visible cluster concentration on the ratio of clusters considered to be <100> loops. As expected, the total concentration decreases as the percentage decreases, without any significant change in the dose dependence. As mentioned above, experimentally visible clusters are only observed for doses above 10^{16}m^{-2}. For the case of pure Fe, concentrations are below 10^{15}m^{-2} for the highest doses studied. The ratio of <100> to $\frac{1}{2}$<111> loops transformed from small SIA loops used in these simulations is 0.1%. This transformation ratio is a parameter that has been adjusted to match experimental data and the information from Figure 1b. It was chosen so that the simulation results agree with experimental measurements of visible cluster concentration for UHP Fe(100) for a thickness of 25 nm as shown below (Figure 8a). Nevertheless, for this comparison, higher values would only increase even more the difference between the two models for this particular condition, that is, thin films.

Figures 2a and 2b present the areal distribution of the loops in the simulation box, projected over the thickness of the thin film as observed from the front surface, for the reaction (Figure 2a) and nucleation (Figure 2b) models, separately, after a radiation dose

of 8.0×10^{17} ions/m^2. This is similar to what would be observed under TEM, except that here defects of all sizes are shown, and not only visible ones. Disks formed by white dots correspond to <100> loops while dark dots are vacancies and small SIA clusters. In the case of the reaction model a threshold of 40 SIA is considered, while for the nucleation model the results for a ratio of 1 immobile <100> loop every 1000 transitions of small SIA clusters are represented. Histograms representing the self-interstitial cluster sizes for these two cases are shown in Figures 2c and 2d. The main difference between the two models is clearly seen in these figures: the reaction model shows very low concentrations of <100> loops with discrete sizes whereas the nucleation model shows higher concentrations and more spread in terms of size ranges. Note that some of the loops have their plane perpendicular to the surface and they appear as a line (a zoom of one of these loops is shown in Figure 2a).

In these simulations, only <100> loops remain in the thin film, due to the recombination of the 1D migrating $\frac{1}{2}$<111> loops with the surfaces. Experimentally, however, even in the ultra-high pure Fe samples, both $\frac{1}{2}$<111> and <100> loops are observed, although the <100> loops represent 86% of the total, which is high but less than the 100% that corresponds to Figures 1 and 2. One possible explanation, as discussed in the introduction, is the trapping of self-interstitial loops by carbon-vacancy or other carbon-interstitial complexes (or equivalent contributions from other interstitial impurities). Therefore, we have considered different trap concentrations. In the following results both nucleation and reaction models for <100> loop formation are allowed in the simulations. A threshold value for the resulting <100> loop of 40 SIA is considered for the reaction model, following the proposal of Marian et. al [39], and a ratio of formation of <100> of 1 every 1000 transformations of small clusters for the nucleation model. These values have been selected so that the concentration of visible <100> clusters is similar to those measured experimentally under these irradiation conditions. The concentration of visible $\frac{1}{2}$<111> loops will be given by the concentration of carbon in bulk due to trapping, as discussed next.

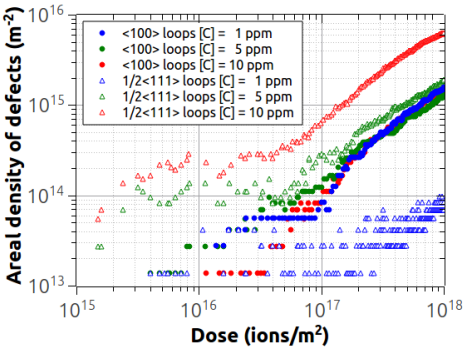

Figure 3: Areal density of $\frac{1}{2}$<111> and <100> loops obtained for different carbon concentrations when both reaction and nucleation models are activated. The simulation volume was set to $270\times270\times50$ nm^3.

Figure 3 shows the results of the simulations for different concentrations of carbon: 1, 5 and 10 ppm (i.e. 5, 23 and 47 appm respectively), including the visible concentration

of <100> and $\frac{1}{2}$<111> loops as a function of dose. As can be appreciated in this figure, the areal density of <100> loops is about the same for all the carbon concentrations evaluated, meanwhile the areal densities of $\frac{1}{2}$<111> loops are highly dependent on carbon concentration. Trapped $\frac{1}{2}$<111> loops are barely present for 1 ppm of carbon, whereas $\frac{1}{2}$<111> and <100> loops are about the same levels of concentrations for 5 ppm, as it can be appreciated in Figure 3. Lastly, the areal density of $\frac{1}{2}$<111> loops is much higher than the concentration of <100> loops when the bulk concentration of carbon is 10 ppm. This is more clearly seen in the histogram of SIA cluster sizes, as shown in Figure 4, where it can be seen that the dominant population of SIA loops is reversed as the carbon concentration in the bulk is increased. For the conditions presented in Figure 4, for 1 ppm C and 50 nm thickness of the foil most of the loops are of <100>. For 5 ppm carbon, the concentration is about the same for both loops, while a clear inversion of the population is obtained for a carbon concentration of 10 ppm, and this is the case for both doses presented here. Note that this behavior is independent of the model for the formation of <100> loops, that is, the inversion of the population is due to trapping of the <111> loops by carbon.

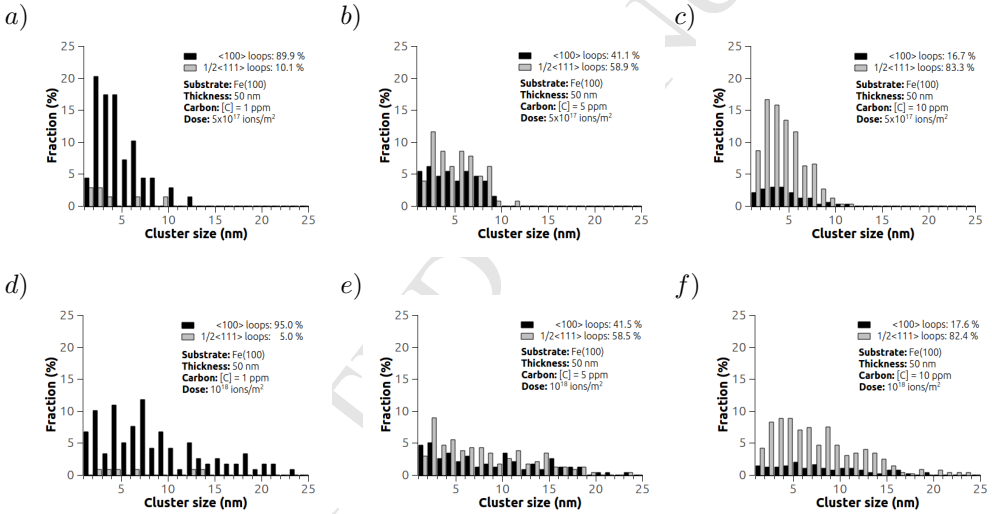

Figure 4: Visible loop size distributions obtained for different carbon concentrations (1, 5 and 10 ppm) when both reaction and nucleation models are activated. Histograms in the upper row are obtained after a dose of 5×10^{17} ions/m^2 while histograms in the lower row were obtained after 10^{18} ions/m^2.

Several aspects of the experimental conditions can thus affect the total concentration of visible clusters measured by TEM, which should be taken into account when comparing to simulation results. The thickness of the irradiated sample is particularly important, as noted by Yao et al [6]. The same authors also mention that the crystal orientation could have an impact on the total visible cluster concentration measured experimentally. Therefore, simulations were performed for different thicknesses of the irradiated sample, from 15 nm up to 85 nm, as shown in Figures 5a and b where the total concentration of visible SIA clusters is represented, as well as different orientations, (100) and (111) (figures (a) and (b) respectively). This particular case corresponds to a carbon concen-

tration of 3 ppm. As the sample thickness decreases, so does the defect concentration. This is a result of the recombination of mobile SIA with surfaces, which is enhanced for thinner samples. As the sample thickness increases, this trend starts to saturate at about 50 nm, as can be noticed from Figures 5a and b. This saturation is due to the depth of the cascade damage for this energy, which hardly reaches 50 nm as obtained from MD calculations [35]. In the experimental work of Yao et. al [6], they observe a gradual fall-off in the areal concentration with foil thickness, which they attribute to a lower visibility of small loops in thick foils, obtained from TEM image simulations [47]. Areal density differences with sample thickness are more clearly seen in the top view of the simulations for a given dose. Figure 6 shows three sample thicknesses, 15 nm, 37 nm and 85 nm, for two different orientations (100) top and (111) bottom figures, and for a total dose of 10^{18} ions/m^2. The upper row in Figure 6 shows the top view of the thin foils with substrate orientation (100), where one may notice that those <100> loops with Burger's vector along [010], [0$\bar{1}$0], [001] and [00$\bar{1}$] directions are hardly visible, as they are perpendicular to the depicted images. Lastly, the corresponding histograms of SIA clusters are represented in Figure 7.

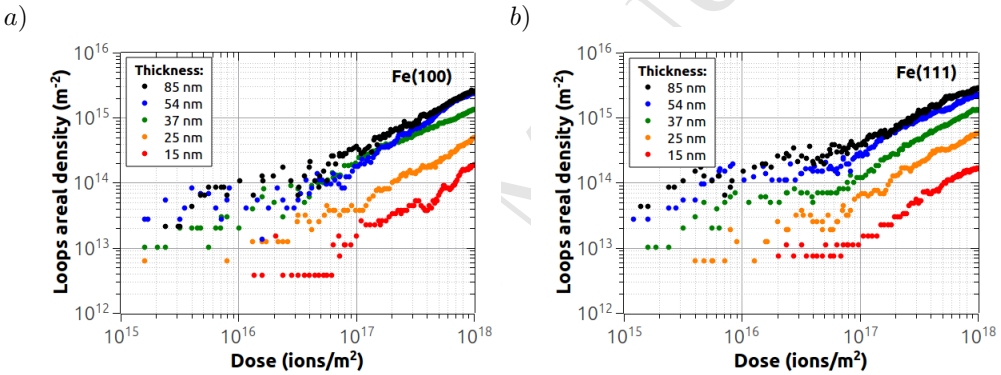

Figure 5: Areal density of visible loops as a function of the irradiation dose and foil thickness for two different substrate orientations (a) Fe(100) and (b) Fe(111). The carbon concentration was set to 3 ppm, and both reaction and nucleation models were activated.

4. Discussion

From the analysis above, it is clear that a quantitative comparison of the model with experimental measurements must be done with caution when considering only visible cluster concentration. The simulations above show that the total visible cluster concentration measured depends strongly on actual sample thickness and carbon content, while the dependence with crystal orientation does not seem to be particularly important for the total defect density. In essence, this means that the main parameter affecting the loop ratio is the mobility and thus the rate of removal of the $\frac{1}{2}$<111> loops. These simulations also show that the reaction model, under the experimental conditions studied here, that is, damage close to the surface and thin samples, is very inefficient for the production of <100> loops due to the fast recombination of $\frac{1}{2}$<111> loops with the surfaces.

Therefore, the nucleation model is needed in order to reproduce the experimental observations. In other words, the picture that emerges is that a small fraction of <100> loops is indeed produced directly upon growth of non-parallel, C15 type interstitial cluster configurations, and they are hardly mobile; some of them may also be produced by reaction between $\frac{1}{2}$<111> loops. If the conditions are such that all the highly mobile $\frac{1}{2}$<111> loops are removed, then all or most visible loops will be of <100> type; otherwise, a more or less small/high ratio of <100> over $\frac{1}{2}$<111> different from 1 will be observed, which will be an indirect index of the effective mobility that impurity concentration and irradiation conditions (e.g. thickness of the specimen, but also temperature, etc.) allow for the $\frac{1}{2}$<111> loops.

Figure 8 shows a comparison of the visible cluster concentration as a function of dose together with the experimental measurements. The parameters for the simulations are those that optimize the comparison to the experiment, that is, minimum size for <100> loop formation of 40 defects for the reaction model and a ratio of 1 every 1000 for the transformation of small SIA clusters to <100> loops for the nucleation model. In both cases the carbon concentration is 3 ppm, following the experimental conditions in Yao et al. [6]*

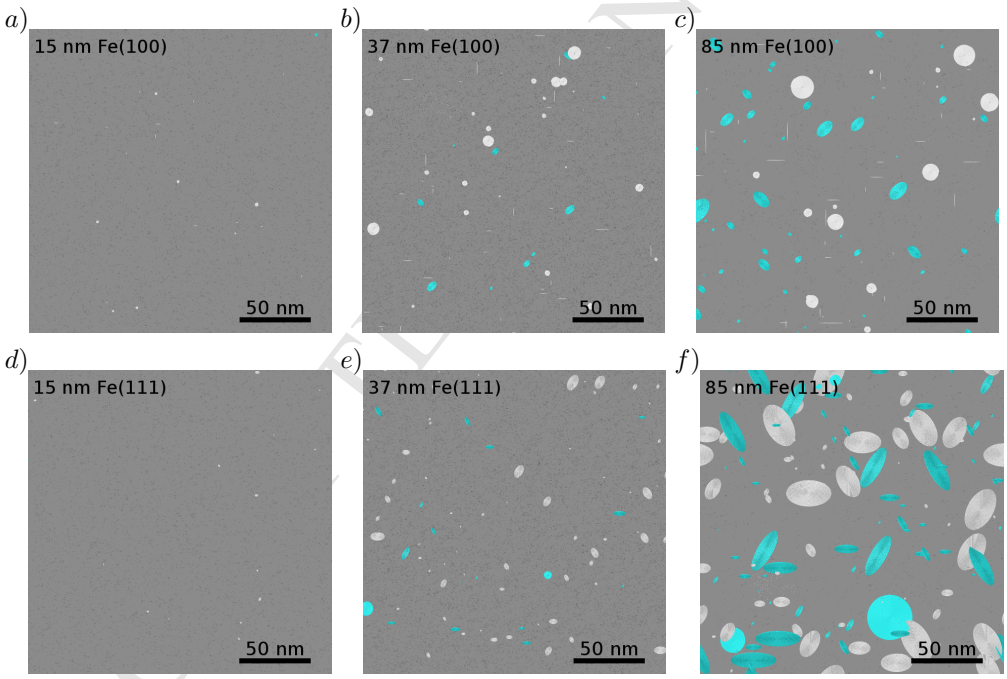

Figure 6: Top view of the graphical representation of defects for both reaction and nucleation models after irradiation for different foil thicknesses. The irradiation dose of these images corresponds to 10^{18} ions/m^2, and the carbon concentration in these simulations was 3 ppm. Disks formed by white dots correspond to <100> loops, while those formed by light blue dots correspond to $\frac{1}{2}$<111> loops.

* In [6] a carbon concentration of 130 ppm is mentioned. However, the purities of the samples used in the experiments were 5N and 4N$^+$, as also indicated in the same article.

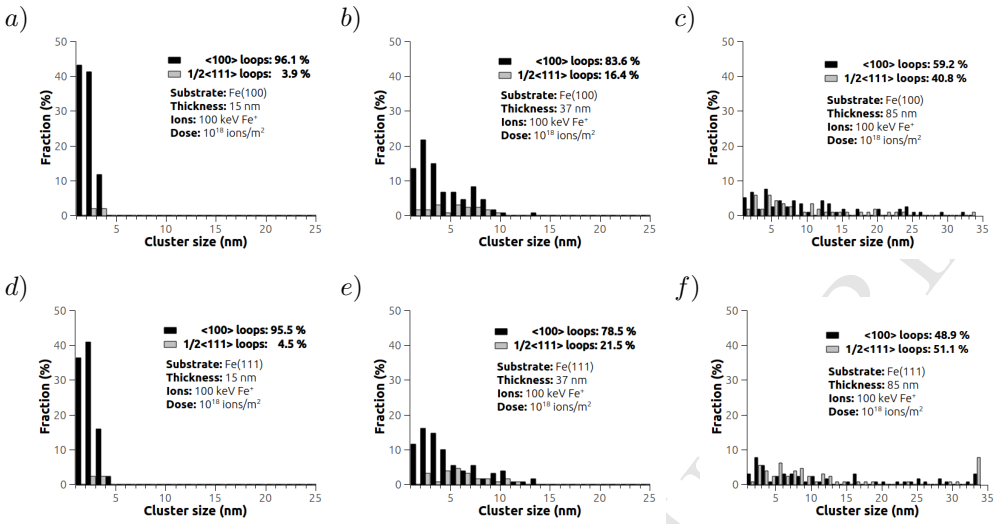

Figure 7: Visible loop size distributions for both reaction and nucleation models after irradiation for different foil thicknesses. The irradiation dose of these histograms corresponds to 10^{18} ions/m^2, and the carbon concentration in these simulations was 3 ppm.

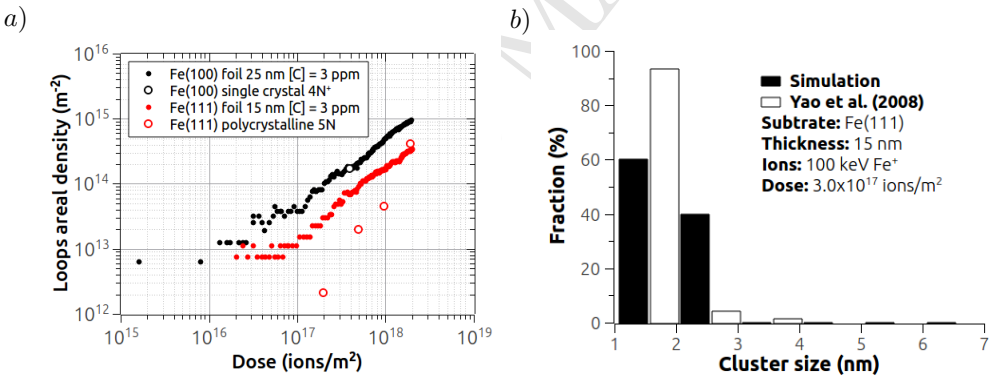

Figure 8: Comparison between the simulated data using both <100> growth models with experimental values from Yao et al. [6]. The filled circles in *a*) correspond to the total visible SIA dislocation loops as a function of the irradiation dose, while the experimental measurements are represented by rings. The histograms depicted in *b*) show the size distribution of loops after a dose of 3×10^{17} ions/m^2 for the substrate Fe(111) polycrystalline 5N in comparison with simulation results.

Calculations for two different crystal orientations (100) and (111) have also been performed, both presented in Figure 8a. Although there is a slight difference between the two orientations, with lower concentrations for the (111) orientation, in agreement with the experimental results, this difference is much smaller than that observed experimentally. This result seems to indicate that the interaction of the mobile interstitials with the surface should be stronger than what has been considered in the model. Currently, defects interact with the surface only when they are located within a distance equal to

a jump distance, 0.287 nm. However, due to image forces [21] the interaction of the surface with loops could be of much longer range, thereby enhancing disappearance of loops, in particular for the (111) orientation. Moreover, the presence of a nearby grain boundary could explain that strong decrease in the loop density for the (111) case. The histograms in Figure 8b are obtained after a dose of 3×10^{17} ions/m^2 for the substrate with orientation (111). It shows a small increase in the averaged size of the visible loops, resulting 1.6 ± 0.2 nm for the experiments of Yao et al. [6] and 1.9 ± 0.3 nm for the simulation results.

5. Conclusions

Through kinetic Monte Carlo simulations and parameters obtained both from classical molecular dynamics simulations and density functional theory, we have studied microstructure evolution in irradiated Fe including the formation of both <100> and $\frac{1}{2}$<111> through two different mechanisms: the nucleation model and the reaction model. The models have been contrasted to TEM characterizations of Fe 100 keV irradiation of Fe thin films. From this comparison we conclude that a fraction of the visible <100> loops are produced directly in the cascade or from C15 type of clusters. The formation of <100> loops from reactions between $\frac{1}{2}$<111> loops is also possible, however, under the conditions in these particular experiments where surfaces play a strong role, due to the film thickness and low carbon concentration, this mechanism is not very efficient. These simulations show that the ratio of <100> to $\frac{1}{2}$<111> loops is very dependent on the efficiency of transport of $\frac{1}{2}$<111> loops to sinks and therefore, it will strongly depend on the irradiation conditions and sample characteristics, particularly sample thickness and impurity content.

Although the exact values of concentrations or ratios could change depending on the parameters in the model, some general and important conclusions emerge from this study. Firstly, the comparison to experimental measurements of defect concentrations obtained with TEM must be done with caution. Several factors influence the concentration of defects observed. Besides carbon concentration or the visibility limit, which has been pointed out by several authors before, this work shows that the thickness of the sample, something that is not always available from the experiments, also plays an important role. Secondly, as already mentioned, the concentration of carbon not only influences the total concentration of visible defects but also the ratio of $\frac{1}{2}$<111> to <100> loops. In fact, this could be a way of validating this model, by systematic studies of irradiated Fe under different carbon concentrations. Finally, the orientation of the crystal sample does not seem to have an important influence in the total defect concentration, although it could give rise to differences in the cluster size distribution. Based on these simulations we propose several ways of validating this model: systematic studies of ion implantation of iron at low energies and different carbon concentrations and crystal orientations.

Acknowledgements

We thank Sergei Dudarev and Robin Schäublin for fruitful discussions. This work has been carried out within the framework of the EUROfusion Consortium and has received funding from the Euratom research and training programme 2014-2018 under

grant agreement No 633053. The views and Opinions expressed herein do not necessarily reflect those of the European Commission. The research leading to these results is partly funded by the European Atomic Energy Communitys (Euratom) Seventh Framework Programme FP7/2007-2013 under grant agreement No. 604862 (MatISSE project) and in the framework of the EERA (European Energy Research Alliance) Joint Programme on Nuclear Materials.

Data availability

The raw data required to reproduce these findings are available to download from Mendeley Data with the identifier http://dx.doi.org/10.17632/2rxrbjcbcv.1

References

[1] B. C. Masters, Dislocation loops in irradiated iron, Nature 200 (1963) 254. doi:10.1038/200254a0.
[2] M. L. Jenkins, C. C. English, B. L. Eyre, Heavy-ion damage in alpha fe, Nature 263 (1976) 400–401. doi:10.1038/263400a0.
[3] B. L. Eyre, Transmission electron microscopy studies of point defect clusters in fcc and bcc metals, Journal of Physics F: Metal Physics 3 (1973) 422–470. doi:10.1088/0305-4608/3/2/009.
[4] B. L. Eyre, Defects in refractory metals, Proceedings of Conf. Mol., Belgium: SCK-CEN (1973) 311.
[5] E. A. Little, R. Bullough, M. H. Wood, On the swelling resistance of ferritic steels, Proceedings of the Royal Society of London Series A: Mathematical Physical and Engineering Sciences 372 (1751) (1980) 565–579.
URL http://www.jstor.org/stable/2397051
[6] Z. Yao, M. Hernandez-Mayoral, M. L. Jenkins, M. A. Kirk, Heavy-ion irradiations of fe and fe-cr model alloys part 1: Damage evolution in thin-foils at lower doses, Philosophical Maganize 88 (2008) 2851. doi:10.1080/14786430802380469.
[7] M. Hernandez-Mayoral, Z. Yao, M. L. Jenkins, M. A. Kirk, Heavy-ion irradiations of fe and fe-cr model alloys part 2: Damage evolution in thin-foils at higher doses, Philosophical Maganize 88 (2008) 2881. doi:10.1080/14786430802380477.
[8] B. L. Eyre, R. Bullough, On the formation of interstitial loops in b.c.c. metals, Journal of Applied Physics 12 (115) (1965) 31–39. doi:10.1080/14786436508224943.
[9] R. Bullough, 15th anniversary of the concept of dislocation in crystals, The Institute of Metals, London (1984) 283.
[10] S. L. Dudarev, R. Bullough, P. M. Derlet, Effect of the $\alpha-\gamma$ phase transition on the stability of dislocation loops in bcc iron, Phys. Rev. Lett. 100 (2008) 135503. doi:10.1103/PhysRevLett.100.135503.
URL https://link.aps.org/doi/10.1103/PhysRevLett.100.135503
[11] D. J. Bacon, F. Gao, Y. N. Osetsky, The primary damage state in fcc, bcc and hcp metals as seen in molecular dynamics simulations, Journal of Nuclear Materials 276 (1–3) (2000) 1–12. doi:10.1016/S0022-3115(99)00165-8.
[12] B. D. Wirth, G. R. Odette, D. Maroudas, G. E. Lucas, Dislocation loop structure, energy and mobility of self-interstitial atom clusters in bcc iron, Journal of Nuclear Materials 276 (2000) 33–40. doi:10.1016/S0022-3115(99)00166-X.
[13] N. Soneda, T. Diaz de La Rubia, Migration kinetics of the self-interstitial atom and its clusters in bcc Fe, Philosophical Magazine, Part A 81 (2001) 331–343. doi:10.1080/01418610130001223 7.
[14] S. L. Dudarev, The non-Arrhenius migration of interstitial defects in bcc transition metals, Comptes Rendus Physique 9 (2008) 409–417. doi:10.1016/j.crhy.2007.09.019.
[15] K. Arakawa, K. Ono, M. Isshiki, K. Mimura, M. Uchikoshi, H. Mori, Observation of the One-Dimensional Diffusion of Nanometer-Sized Dislocation Loops, Science 318 (2007) 956. doi:10.1126/science.1145386.
[16] M. J. Caturla, N. Soneda, E. Alonso, B. D. Wirth, T. Díaz de la Rubia, J. M. Perlado, Comparative study of radiation damage accumulation in Cu and Fe, Journal of Nuclear Materials 276 (2000) 13–21. doi:10.1016/S0022-3115(99)00220-2.

[17] Y. Satoh, H. Matsui, T. Hamaoka, Effects of impurities on one-dimensional migration of interstitial clusters in iron under electron irradiation, Physical Review B 77 (9) (2008) 094135. doi:10.1103/PhysRevB.77.094135.
[18] N. Anento, A. Serra, Carbon-vacancy complexes as traps for self-interstitial clusters in Fe-C alloys, Journal of Nuclear Materials 440 (2013) 236–242. doi:10.1016/j.jnucmat.2013.04.087.
[19] D. Terentyev, I. Martin-Bragado, Evolution of dislocation loops in iron under irradiation: The impact of carbon, Scripta Materialia 97 (2015) 5–8. doi:10.1016/j.scriptamat.20141.00.21.
[20] C. Barouh, T. Schuler, C.-C. Fu, M. Nastar, Interaction between vacancies and interstitial solutes (C, N, and O) in α-Fe From electronic structure to thermodynamics, Physical Review B 90 (5) (2014) 054112. doi:10.1103/PhysRevB.90.054112.
[21] A. Prokhodtseva, B. Décamps, R. Schäublin, Comparison between bulk and thin foil ion irradiation of ultra high purity Fe, Journal of Nuclear Materials 442 (2013) S786–S789. doi:10.1016/j.jnucmat.2013.04.032.
[22] C. Domain, C. S. Becquart, Solute - <111> interstitial loop interaction in α-Fe: A DFT study, Journal of Nuclear Materials 499 (2018) 582–594. doi:10.1016/j.jnucmat.2017.10.070.
[23] J. Marian, B. D. Wirth, J. M. Perlado, Mechanism of Formation and Growth of <100> Interstitial Loops in Ferritic Materials, Physical Review Letters 88 (25) (2002) 255507. doi:10.1103/PhysRevLett.88.255507.
[24] H. Xu, R. E. Stoller, Y. N. Osetsky, D. Terentyev, Solving the Puzzle of <100> Interstitial Loop Formation in bcc Iron, Physical Review Letters 110 (26) (2013) 265503. doi:10.1103/PhysRevLett.110.265503.
[25] G. J. Ackland, M. I. Mendelev, D. J. Srolovitz, S. Han, A. V. Barashev, Development of an interatomic potential for phosphorus impurities in α-iron, Journal of Physics: Condensed Matter 16 (27) (2004) S2629–S2642. doi:10.1088/0953-8984/16/27/003.
[26] L. Malerba, M. C. Marinica, N. Anento, C. Björkas, H. N. C. Domain, F. Djurabekova, P. O. K. Nordlund, A. Serra, D. Terentyev, F. Willaime, C. S. Becquart, Comparison of empirical interatomic potentials for iron applied to radiation damage studies, Journal of Physics: Condensed Matter 406 (2010) 19–38. doi:10.1016/j.jnucmat.2010.05.017.
[27] M.-C. Marinica, F. Willaime, J.-P. Crocombette, Irradiation-Induced Formation of Nanocrystallites with C15 Laves Phase Structure in bcc Iron, Physical Review Letters 108 (2) (2012) 025501. doi:10.1103/PhysRevLett.108.025501.
[28] D. A. Terentyev, T. P. C. Klaver, P. Olsson, M.-C. Marinica, F. Willaime, C. Domain, L. Malerba, Self-Trapped Interstitial-Type Defects in Iron, Physical Review Letters 100 (14) (2008) 145503. doi:10.1103/PhysRevLett.100.145503.
[29] Y. Zhang, X.-C. Bai, M. R. Tonks, B. Biner, Formation of prismatic loops from c15 laves phase interstitial clusters in body-centered cubic iron, Scripta Materialia 98 (2015) 5–8. doi:10.1016/j.scriptamat.2014.10.033.
[30] C. Domain, C. S. Becquart, L. Malerba, Simulation of radiation damage in Fe alloys: an object kinetic Monte Carlo approach, Journal of Nuclear Materials 335 (2004) 121–145. doi:10.1016/j.jnucmat.2004.07.037.
[31] A. Hardouin Duparc, C. Moingeon, N. Smetniansky-de-Grande, A. Barbu, Microstructure modelling of ferritic alloys under high flux 1 MeV electron irradiations, Journal of Nuclear Materials 302 (2002) 143–155. doi:10.1016/S0022-3115(02)00776-6.
[32] V. Jansson, M. Chiapetto, L. Malerba, The nanostructure evolution in Fe-C systems under irradiation at 560 K, Journal of Nuclear Materials 442 (2013) 341–349. arXiv:1407.7215, doi:10.1016/j.jnucmat.2013.09.017.
[33] D. Terentyev, N. Anento, A. Serra, V. Jansson, H. Khater, G. Bonny, Interaction of carbon with vacancy and self-interstitial atom clusters in α-iron studied using metallic-covalent interatomic potential, Journal of Nuclear Materials 408 (2011) 272–284. doi:10.1016/j.jnucmat.2010.11.053.
[34] D. Terentyev, K. Heinola, A. Bakaev, E. E. Zhurkin, Carbon-vacancy interaction controls lattice damage recovery in iron, Scripta Materialia 86 (2014) 9–12. doi:10.1016/j.scriptamat.2014.04.003.
[35] M. J. Aliaga, R. Schäublin, J. F. Löffler, M. J. Caturla, Surface-induced vacancy loops and damage dispersion in irradiated fe thin films, Acta Materialia 101 (2015) 22–30. doi:10.1016/j.actamat.2015.08.063.
[36] I. Martin-Bragado, A. Rivera, G. Valles, J. L. Gomez-Selles, M. J. Caturla, Mmonca: An object kinetic monte carlo simulator for damage irradiation evolution and defect diffusion, Computer Physics Communications 184 (2013) 2703–2710. doi:10.1016/j.cpc.2013.07.011.
URL `https://github.com/spartankel/MMonCa`
[37] C.-C. Fu, J. Dalla Torre, F. Willaime, J.-L. Bocquet, A. Barbu, Multiscale modelling of defect

kinetics in irradiated iron, Nature Materials 4 (2005) 68–74. doi:10.1038/nmat1286.

[38] F. Willaime, C.-C. Fu, M.-C. Marinica, J. Dalla Torre, Stability and mobility of self-interstitials and small interstitial clusters in α-iron: ab initio and empirical potential calculations, Nuclear Instruments and Methods in Physics Research B 228 (2005) 92–99. doi:10.1016/j.nimb.2004.10.028.

[39] J. Marian, B. D. Wirth, R. Schäublin, G. R. Odette, J. M. Perlado, MD modeling of defects in Fe and their interactions, Journal of Nuclear Materials 323 (2003) 181–191. doi:10.1016/j.jnucmat.2003.08.037.

[40] M. R. Gilbert, S. L. Dudarev, P. M. Derlet, D. G. Pettifor, Structure and metastability of mesoscopic vacancy and interstitial loop defects in iron and tungsten, Journal of Physics Condensed Matter 20 (2008) 345214. doi:10.1088/0953-8984/20/34/345214.

[41] N. Soneda, T. Diaz de La Rubia, Defect production, annealing kinetics and damage evolution in alpha-Fe: an atomic-scale computer simulation, Philosophical Magazine, Part A 78 (1998) 995–1019. doi:10.1080/01418619808239970.

[42] D. R. Mason, X. Yi, M. A. Kirk, S. L. Dudarev, Elastic trapping of dislocation loops in cascades in iron-irradiated tungsten foils, Journal of Physics: Condensed Matter 26 (2014) 375701. doi:10.1088/0953-8984/26/37/375701.

[43] F. Ferroni, E. Tarleton, S. Fitzgerald, Dislocation dynamics modelling of radiation damage in thin films, Modelling and Simulation in Materials Science and Engineering 22 (4) (2014) 045009. doi:10.1088/0965-0393/22/4/045009.

[44] W. Wu, Free surface effects in tem imaging of dislocation lines and loops in fe, Ph.D. thesis, École Polytechnique Fédérale de Lausanne (June 2014).

[45] M. Wen, N. Ghoniem, B. Singh, Kinetic Monte Carlo simulations of dislocation decoration and raft formation in bcc-iron under cascade irradiation, Vol. DOE/ER-0313/35, 2004, pp. 201–208.

[46] V. Jannson, Radiation-induced nanostructure evolution models for fe alloys, Ph.D. thesis, University of Helsinki, Faculty of Science, Department of Physics, Division of Materials Physics (dec 2013). URL `http://hdl.handle.net/10138/42196`

[47] Z. Zhou, M. L. Jenkins, S. L. Dudarev, A. P. Suttons, M. A. Kirk, Simulations of weak-beam diffraction contrast images of dislocation loops by the many-beam howie-basinski equations, Philosophical Maganize 86 (2006) 4851–4881. doi:10.1080/14786430600615041.